IOPscience iopscience.iop.org

Home Search Collections Journals About Contact us My IOPscience

Theory of persistent, p-type, metallic conduction in c-GeTe

This article has been downloaded from IOPscience. Please scroll down to see the full text article.

2005 J. Phys.: Condens. Matter 17 L329

(http://iopscience.iop.org/0953-8984/17/32/L01)

View the table of contents for this issue, or go to the journal homepage for more

Download details:
IP Address: 129.252.86.83
The article was downloaded on 28/05/2010 at 05:49

Please note that terms and conditions apply.

INSTITUTE OF PHYSICS PUBLISHING JOURNAL OF PHYSICS: CONDENSED MATTER

J. Phys.: Condens. Matter **17** (2005) L329–L335 doi:10.1088/0953-8984/17/32/L01

LETTER TO THE EDITOR

Theory of persistent, p-type, metallic conduction in c-GeTe

Arthur H Edwards[1], Andrew C Pineda[1], Peter A Schultz[2], Marcus G Martin[2], Aidan P Thompson[2] and Harold P Hjalmarson[2]

[1] Air Force Research Laboratory, Space Vehicles Directorate, 3550 Aberdeen Avenue SE, KAFB, NM 87117-5776, USA
[2] Multiscale Computational Materials Methods, Sandia National Laboratories, PO Box 5800, MS 1110, Albuquerque, NM 87185-1110, USA

Received 28 June 2005
Published 29 July 2005
Online at stacks.iop.org/JPhysCM/17/L329

Abstract

It has been known for over twenty years that rhombohedral c-germanium telluride is predicted to be a narrow gap semiconductor. However, it always displays p-type metallic conduction. This behaviour is also observed in other chalcogenide materials, including $Ge_2Sb_2Te_5$, commonly used for optically and electrically switched, non-volatile memory, and so is of great interest. We present a theoretical study of the electronic structure of the perfect crystal and of the formation energies of germanium/tellurium vacancy and antisite defects in rhombohedral germanium telluride. We find that germanium vacancies are by far the most readily formed defect, independent of Fermi level and of growth ambient. Moreover, we predict that the perfect crystal is thermodynamically unstable. Thus, the predicted large equilibrium densities of the germanium vacancy of $\sim 5 \times 10^{19}$ cm^{-3} results in a partially filled valence band and in the observed p-type conductivity.

1. Introduction

For over thirty years switching has been observed between high and low conductivity states in a variety of chalcogen-based alloys [1–3]. Many chalcogenide systems switch between these two states within tens of nanoseconds when exposed to laser light or to electrical current. However, upon thermal heating, the transition can take minutes [4], implying that the laser- and electrically induced phase transition depends on electronic transport. There have been several studies of the electronic structure of crystalline [5, 6] and amorphous [7, 8] phases. All calculations of the perfect rhombohedral material predict a band gap between 0.4 eV [6] and 0.7 eV [9]. However, transport studies indicate that the polycrystalline material is metallic [1]. The dominant carriers are observed to be holes. This is a troubling discrepancy between theory and experiment because, to date, theory cannot predict even qualitative observations

 © 2005 IOP Publishing Ltd Printed in the UK

in GeTe. Furthermore, persistent p-type conductivity is observed in other chalcogenide-based alloys, including $Ge_2Sb_2Te_5$, the most commonly used alloy for both optically and electrically switched non-volatile memory.

In this letter, we report the first cogent theoretical explanation of the apparent contradiction between theory and the observed free-carrier transport. We use density functional theory (DFT) calculations to show that the p-type metallic character is the result of a large equilibrium concentration of the germanium vacancy. We calculate the conformation, electronic structure, and formation energies of the vacancy and antisite defects in the low-temperature, rhombohedral phase of crystalline germanium telluride (space group $R3m$). We then focus on the material's behaviour induced by the germanium vacancy, by far the most easily formed intrinsic defect.

Our DFT calculations were performed with QUEST, which employs a well converged Gaussian local orbital basis (double-zeta with polarization). We used the local density approximation, the Perdew–Zunger parameterization [10] of the Ceperly–Alder free-electron exchange correlation potential [11], and Hamann pseudopotentials [12]. We used Monkhorst–Pack (MP) k-grids [13] of varying sizes for different unit cells. We show elsewhere [9] that our results are converged with respect to k-point sampling and to numerical grid spacing. For the defect calculations, we used three different supercell sizes containing 64, 128, and 250 atoms. The 64-atom cell was built from an 8-atom non-primitive cell, while the 128- and 250-atom cells were built from the 2-atom primitive cell. We used a $3 \times 3 \times 3$ MP k-grid in the two smaller unit cells, and a $2 \times 2 \times 2$ MP k-grid in the largest supercell. For the two larger supercells, this k-gridding is equivalent to $12 \times 12 \times 12$ and $9 \times 9 \times 9$ k-grids in the primitive rhombohedral cell. Because the smallest supercell was derived from a non-primitive cell, there is no strict equivalence to gridding in the primitive cell. However, the density of k-points is greater than for a $9 \times 9 \times 9$ gridding in the primitive cell.

We calculated the electrical levels using

$$E(n-1/n) = E_{\mathrm{d}}(n-1) + E_{\mathrm{p}}(n) - E_{\mathrm{d}}(n) - E_{\mathrm{p}}(n-1), \tag{1}$$

where E_{p} (E_{d}) refers to the total energy of the perfect (defective) unit cell. With this definition, the reference for the electrical levels depends on the sign of the charge state(s) involved. For $n-1$ less than (greater than or equal to) zero the reference is the conduction (valence) band edge.

We calculated the formation energies for defects using two methods. The first is the standard relationship for highly localized defects:

$$E_{\mathrm{form}}(q) = E_{\mathrm{d}}(q) - E_{\mathrm{p}}(q=0) - \sum_{i=1}^{\mathrm{n\ type}} (N_i \mu_i) + q\epsilon_{\mathrm{F}}. \tag{2}$$

The second follows a prescription analogous to equation (1):

$$E_{\mathrm{form}}(q) = E_{\mathrm{d}}(q) - E_{\mathrm{p}}(q) - \sum_{i=1}^{\mathrm{n\ type}} (N_i \mu_i) + q\epsilon_{\mathrm{F}}, \tag{3}$$

where μ_i is the chemical potential for the reservoir of type i atoms, and N_i is the number of type i atoms added to (>0) or removed from (<0) the perfect system to make the defect. Both of these prescriptions can account for different growth ambients [14]. We calculated formation energies for Te-rich and Ge-rich environments and for the case where both reservoirs are available. The standard states for the Ge and Te reservoirs are the respective elemental solids. Equations (2) and (3) are identical for the neutral charge state. In equation (3), the zero of energy is given by the last occupied state in the perfect supercell. Hence, for the $-/0$ charge state, we have to subtract an effective band gap energy to align the formation energies. For both

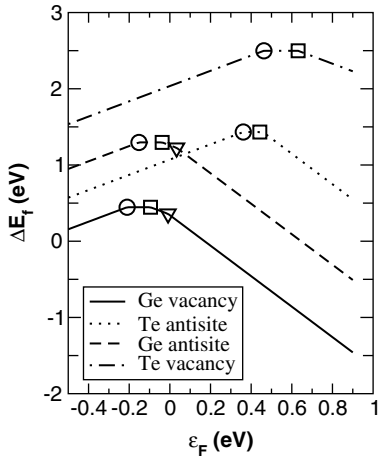

Figure 1. Calculated electrical levels (symbols) and formation energies, for germanium-rich growth, as a function of Fermi level, for the intrinsic antisite and vacancy defects. The symbols have the following meanings: ○: 0/+, □: −/0, ▽: =/−. The zero of Fermi energy is at the valence band edge.

prescriptions, we assign the zero of energy as the energy of formation for the stoichiometric supercell cell when the Fermi level is at the valence band edge. For a given defect, the electrical levels and $E_{\rm form}(q)$ at one value of the Fermi energy determine $E_{\rm form}(q)$ for all values of the Fermi energy. Equation (3) gives results for the charged defects that are internally consistent. That is, we can start in any charge state and derive the same formation energy as a function of Fermi energy. This is not true for equation (2), for which the charged results are shifted by a factor that is independent of the defect, but depends on the size of the supercell. As discussed at length elsewhere, this is the result of negligible charge localization for these defects. All energies of formation reported here were calculated using equation (3).

In figure 1 we show the electrical levels (symbols) and the formation energies of the vacancy and antisite defects as a function of Fermi level for a germanium-rich environment. The results are identical qualitatively and similar quantitatively for the other two cases. There are several important features in figure 1. First, all four defects are predicted to have a positive $U_{\rm eff}$ [15]. Second, for the germanium vacancy and the germanium antisite defects, the $0/+$, $-/0$, and $=/-$ electrical levels are all at or below the valence band edge. Third, and most important, the germanium vacancy is, by far, the most readily formed defect at any Fermi level.

In figure 2 we show the local equilibrium structure of the ideal crystal, and of the germanium vacancy. The local geometrical parameters are given in table 1. The crystal is made of sheets of atoms in which each atom has approximately sixfold coordination. However, three neighbours in the same sheet are slightly closer than those in the next sheet. We use the terms intersheet and intrasheet to distinguish the two sets of near neighbours.

The changes in both bond length and bond angle around the vacancy are small, although there is clear reconstruction. Each intrasheet, nearest-neighbour, tellurium atom has an intersheet bond to one germanium atom that is directly opposite the vacancy site.

In figure 3 we show the total density of states (TDOS) for the vacancy superimposed on the TDOS for bulk GeTe. Remarkably, the germanium vacancy introduces no one-electron levels in the forbidden gap. To explore the localization for the germanium vacancy, we calculated

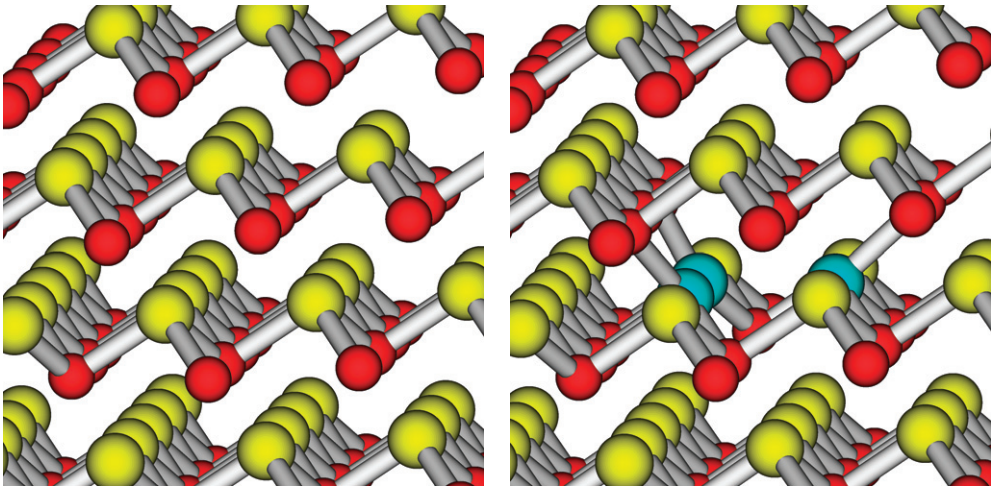

(a) (b)

Figure 2. Geometries of rhombohedral GeTe (a), and of the Ge vacancy (b). Red atoms are germanium, gold are tellurium. For the vacancy, (b), nearest-neighbour Te atoms are blue for clarity.

Table 1. Calculated equilibrium geometries for the germanium vacancy in rhombohedral GeTe for the 128-atom supercell. (nn) indicates the (intrasheet) nearest neighbours to the defect. Primed atoms indicate intersheet distances. The pair of values in parentheses indicates bonded and unbonded intersheet distances. Local geometries for the 128- and 250-atom supercells are nearly identical.

	Perfect	Ge vacancy
$R_{\mathrm{Te(nn)-Ge}}$ (Å)	2.82	2.79
$R_{\mathrm{Te(nn)-Te(nn)}}$ (Å)	4.15	4.08
$R_{\mathrm{Te(nn)-Ge'}}$	3.14	(2.92, 3.11)
∠Ge–Te(nn)–Ge (deg)	94.7	93.7

projected densities of states (PDOS) on the nearest-neighbour tellurium atoms and on the second-nearest-neighbour germanium atoms and compare these to tellurium and germanium atoms in the bulk. There were no significant changes for the germanium atom. However, as shown in figure 4, there are two prominent features in the nearest-neighbour tellurium PDOS that are absent in the perfect crystal: one roughly 0.25 eV below the valence band edge and one very deep (~ -15.2 eV) that is part of the Te s-bands. The PDOS for a Te atom roughly 10 Å away from the vacancy is indistinguishable from the perfect crystalline case. As shown in figure 1, the calculated V_{Ge} 0/+ electrical level is 0.21 eV *below* the valence band edge, consistent with the one-electron PDOS. For all the unit cells containing one Ge vacancy, the Fermi level is *below* the valence band edge. For the neutral germanium vacancy, there is an empty state (two holes) at the top of the valence band. To understand this more fully, we integrated over the density of occupied states for the perfect and the defective superlattices. Removing the germanium atom removes one state from the valence bands, while removing four electrons, thus leaving a completely empty state at the valence band edge. Often localized defects have energy levels that depend on occupation. To explore this possibility, we added

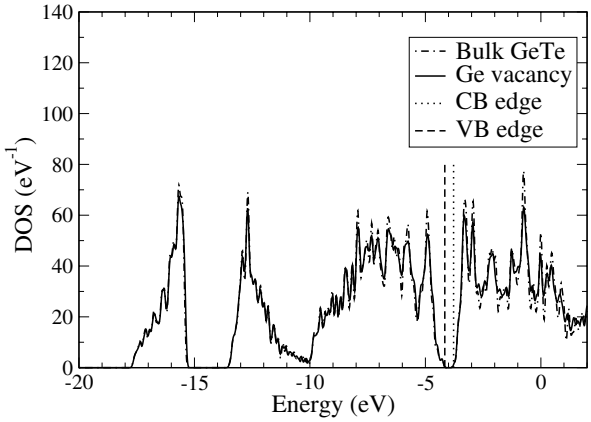

Figure 3. Total density of states (TDOS) for the germanium vacancy superimposed on the TDOS for bulk GeTe.

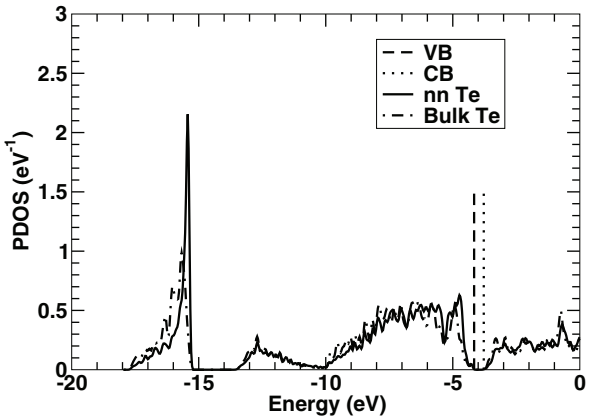

Figure 4. Comparison of projected density of states for a tellurium atom in perfect, $R3m$ GeTe and for the nearest-neighbour tellurium atom for the germanium vacancy.

first one and then two electrons and allowed the system to relax completely. In both cases the added charge induced negligible atomic relaxations. Furthermore, we calculated the TDOS for the germanium vacancy with two electrons added to the system and used Van de Walle's method [14] to align with the eigenstates of the neutral vacancy. There is no discernible difference between these two functions. Finally, we calculated the difference in pseudocharge density on the nearest-neighbour germanium atoms between the neutral and -2 charge states and found it to be consistent with uniform distribution. All of these results are consistent with the extra electrons occupying valence band states that are unperturbed by the defect. Shallow levels can merge with the band edge artificially if the supercell is too small. In fact, for shallow donors and acceptors, the supercell method is inappropriate. We studied the electrical levels as a function of unit cell size and found that the results reported here are qualitatively insensitive. In fact, the $0/+$ electrical level for the germanium vacancy moves deeper into the valence bands for increased unit cell size. So we have the case that the defect state shows localization through the PDOS, but any added charge is purely delocalized.

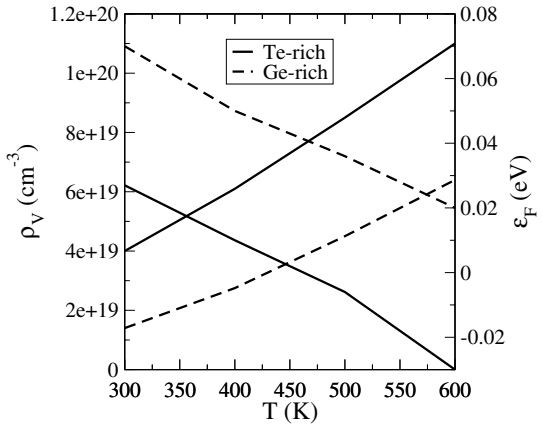

Figure 5. Calculated equilibrium vacancy concentration and Fermi-energy (with respect to the valence band edge) as a function of temperature. Monotonically increasing (decreasing) curves are referenced to the left-hand (right-hand) y-axis.

Significantly, when the Fermi level is near mid-gap, as for the perfect solid, we predict that the germanium vacancy has a negative formation energy. However, a small formation energy at the valence band edge that decreases rapidly as the Fermi level moves upward from the valence band implies that the Fermi level will always be near or below the valence band edge. As discussed in detail in [9], we calculated the Fermi level and vacancy concentrations as a function of temperature. The results are shown in figure 5. For all temperatures, the calculated equilibrium Fermi level is within 0.1 eV of the valence band edge, and there is a large density of holes. For tellurium-rich growth environments, we predict equilibrium vacancy concentrations starting at 4×10^{19} cm^{-3}. This is qualitatively consistent with measurements by Bahl and Chopra [1], although they claim that the Fermi level is inside the valence band by approximately 0.3–0.5 eV. Based on our calculations, this would imply highly non-equilibrium growth conditions, or a significant overestimation of the calculated formation energy for the germanium vacancy.

To conclude, through the first systematic, first-principles study of the vacancy and antisite defects in rhombohedral germanium telluride, we have shown that the electronic structure and, hence, the nature of free carrier transport is determined by the germanium vacancy. It is, by far, the most easily formed of these defects. Because of the electrical-level positions, its formation energy is monotonically decreasing with increasing Fermi levels inside the forbidden gap. Our equilibrium prediction is that the Fermi level is just above the valence band edge, leading to hole concentrations greater than 10^{19} cm^{-3}. This gives a natural explanation for the experimental observation that germanium telluride is always p-type. It also gives a qualitative explanation of the origin of metallic hole conduction. Thus, for this material, a careful study of intrinsic defects has proved essential for restoring confidence in the predictive capacity of electronic structure calculations.

This work was supported through the Air Force Office of Scientific Research, and through the Computer Science Research Foundation of Sandia National Laboratories. Sandia is a multiprogram laboratory operated by Sandia Corporation, a Lockheed Martin Company, for the United States Department of Energy's National Nuclear Security Administration under Contract DE-AC04-94AL85000.

References

[1] Bahl S K and Chopra K L 1970 *J. Appl. Phys.* **41** 2196
[2] Das V D, Soundararajan N and Pattabi M 1987 *J. Mater. Sci.* **22** 3522
[3] Feinleib J and Ovshinsky S R 1970 *J. Non. Cryst. Solids* **4** 564
[4] Lu Q M and Libera M 1995 *J. Appl. Phys.* **77** 517
[5] Cohen M H, Falicov L M and Golin S 1964 *IBM J.* **8** 215–27
[6] Rabe K M and Joannopoulos J D 1987 *Phys. Rev.* B **36** 3319
[7] O'Reilly E P, Robertson J and Kelly M J 1981 *Solid State Commun.* **38** 565
[8] Reilly E P O 1982 *J. Phys. C: Solid State Phys.* **15** 1449
[9] Edwards A H, Schultz P, Pineda A C, Hjalmarson H J, Martin M and Thompson A 2005 unpublished
[10] Perdew J and Zunger A 1981 *Phys. Rev.* B **23** 5048
[11] Ceperly D M and Alder B J 1980 *Phys. Rev. Lett.* **45** 566
[12] Hamann D R 1989 *Phys. Rev.* B **40** 2980
[13] Monkhorst H J and Pack J D 1976 *Phys. Rev.* B **13** 5188
[14] Laks D B, de Walle C G V, Neumark G F, Blöchl P D and Pantelides S T 1992 *Phys. Rev.* B **45** 10965
[15] Anderson P W 1975 *Phys. Rev. Lett.* **34** 953